Desalination and Water Treatment
www.deswater.com

doi: 10.5004/dwt.2019.24771

171 (2019) 408–417
December

Layer-by-layer self-assembled dopamine/PEI fibers derived from *Ceiba pentandra* for the anionic dye adsorption

Fei Chai[a], Runkai Wang[a,*], Pinhua Rao[a], Wenqi Zhang[b], Lili Yan[a], Niannian Yang[a], Yiyun Cai[a], Chunyan Xi[a]

[a]*School of Chemistry and Chemical Engineering, Shanghai University of Engineering Science, No. 333, Longteng Road, Songjiang District, Shanghai 201620, China, Tel. (+86) 021-67791217; emails: wrk007@163.com (R. Wang), cfpbj0501@163.com (F. Chai), raopinhua@sues.edu.cn (P. Rao), lily.502@163.com (L. Yan), yangnn1025@163.com (N. Yang), 645318173@qq.com (Y. Cai), 1393285440@qq.com (C. Xi)*

[b]*College of Civil Engineering, Kashgar University, No. 29, College Road, Kashgar City, Xinjiang 844000, China, Tel. (+86) 021-67791217; email: zhangwenqi@sues.edu.cn*

Received 30 March 2019; Accepted 28 July 2019

ABSTRACT

Aiming to increase the industrial application potential of kapok fibers (KF) derived from *Ceiba pentandra* to deal with the anionic dyes from water, a novel biosorbent with abundant ammonium groups was synthesized via layer-by-layer self-assembly of the surface polymerization of dopamine (DOPA) with cross-linked polyethyleneimine (PEI) and glutaraldehyde (GA). During the self-assembly process of the biosorbent (KF-DOPA-PEI/GA), the response surface methodology based on three-level three-factorial Box–Behnken design was applied to establish the optimum modification conditions. The morphological and surface characterization was carried out with scanning electron microscope, Fourier transform infrared spectroscopy and contact angle measurement demonstrating the successful assembly on the surface of kapok fibers. The batch tests investigated a high adsorption efficiency towards methyl orange (MO) with the maximum adsorption capacity of 85.02 mg/g and the biosorbent showed excellent reusability after five cycles with the hydrochloric acid solution, indicating a potential adsorbent for anionic dyes containing wastewater treatment.

Keywords: *Ceiba pentandra*; Layer-by-layer; Self-assembly; Response surface methodology; Anionic dyes adsorption

1. Introduction

An increased awareness of cost effectiveness and the protection of public and environmental health has focused attention on the development of natural eco-friendly sorbents for wastewater treatment and industrial applications [1–4]. The agricultural product kapok fiber (KF) is derived from the fruits of *Ceiba pentandra*, which is mainly distributed in deciduous forests of western and eastern India, especially in areas with hotter climates [5,6]. After ripening and cracking, the seeds enveloping the KF fall from the plant; approximately 190,000 tons are naturally produced in China annually [7]. However, only a small amount of this KF is collected for use as a filling material for pillows and life jackets [8]. The majority of the fibers drift away in the wind after they reach maturity, which adds to the pollution problem and is considered a waste of a potential bioresource. The reasons behind this limited application include the weak flammability and hydrophobic properties of the fibers [9,10], although the same characteristics have led to their application in

* Corresponding author.

processes such as oil adsorption [11–14], oil-water separation and water-repelling [15,16]. In addition, a KF has a hollow structure and porosity of 80% which is greater than other natural fibers. The fibers also possess low dyeing efficiencies toward hydrophilic coloring agents and dyes [17], which has greatly limited their industrial application. Therefore, the development of a method to improve the functional properties of KF (e.g., wettability) is required to effectively use KF in processes such as the adsorption of metal ions [18,19] and treatment with antibacterial agents [20].

Surface modification is a popular method used to increase the wettability of KF. In early studies, these modifications were conducted using acids and alkalis. Agcaoili et al. [21] fabricated polyacrylonitrile-coated kapok hollow microtubes and found that the wettability of the fibers was reduced in parallel with a drastic increase in hydrophilicity. This modification resulted in enhanced adsorption efficiencies of methyl orange (MO) dye and Cu(II) from an aqueous solution. The biopolymer dopamine (DOPA) facilitates strong attachment onto the substrate through a dismutation reaction. The abundant catechol and imine/amine groups that form in the polydopamine (PDA) structure are thought to improve substrate hydrophilicity and provide active sites for polyethyleneimine (PEI) binding [22–24]. Nevertheless, the cross-linking of DOPA and PEI is unstable due to the poor film-forming ability of PEI. Therefore, glutaraldehyde (GA) has been selected as the cross-linking agent, and found to effectively construct the fully-interpenetrating polymer, thereby enhancing the mechanical properties and dimensional stability of the membranes [25].

In this study, a novel biosorbent (KF-DOPA-PEI/GA) with an abundance of ammonium groups was synthesized via layer-by-layer self-assembly of the surface polymerization of DOPA with cross-linked PEI and GA. During the self-assembly process, the response surface methodology (RSM) [26] was applied to establish the optimum modification conditions. The RSM included the effect of the two-step modification and an investigation into the adsorption properties of KF-DOPA-PEI/GA for anionic contaminants in a MO aqueous solution (a typical acid anionic mono-azo dye [27–29]). Further investigations into basic thermodynamic isotherms, pH effects, kinetic aspects and regeneration were also performed. Additionally, surface characterization regarding morphology and wettability of the modified KF was assessed.

2. Experiment

2.1. Materials

Raw KF was kindly provided by Seohae Environment Science Institute (Jeonju 561-211, Korea). Polyethyleneimine (PEI, MW = 10,000), glutaraldehyde (GA, 25% in water) and 3-hydroxytyramine hydrochloride (DOPA, 99%, MW = 189.64) were purchased from Adamas-beta (No. 245, Jiachuan Road, Shanghai, China). Tris (hydroxymethyl) aminomethane (Tris-HCl) was sourced from Aladdin (No. 809, Chuhua Branch Road, Shanghai, China). MO solutions were prepared in distilled water at room temperature. Other chemical reagents such as NaOH and HCl were all of analytical grade and used as received without further purification.

2.2. Layer-by-layer self-assembly on the surface of KF

As a pre-treatment, the fibers were washed several times in deionized water (DW) to remove impurities, and then dried in a vacuum oven. For the surface modification of KFs, a DOPA solution was prepared in tris-HCl buffer solution (0.01 mol/L, pH 8), into which pretreated KFs were immersed and stirred for 24 h under shade. The surface modified KFs (KF-DOPA) were rinsed with DW and dried. Self-assembly was then initiated by the addition of PEI solution, and stirring KF-DOPA for a set amount of reaction time with a solid–liquid ratio. The rinsed and dried adsorbent (KF-DOPA-PEI) was immersed and stirred in GA solution at 50°C for 1 h to allow the cross-linking process to enhance the dimensional stability of the formed polymer layer. Finally, KF-DOPA-PEI/GA was filtered and washed with distilled water to remove any unreacted chemicals, and dried in a vacuum at 60°C for 24 h.

2.3. Characterization

Fourier transform infrared (FTIR) spectral analyses were carried out in transmission mode using a Thermo Nicolet AVATAR 370 spectrophotometer with KBr pellets. Surface morphologies were observed using a field emission scanning electron microscope (FE-SEM, JSM-6701F). Changes in water contact angle were determined using contact angle measurements (JY-82B).

2.4. RSM assessment

To establish optimum synthesis conditions, the three-level, three-factorial Box–Behnken experimental design with a categoric factor of 0 was employed, based on the MO adsorption capacity of the adsorbents. A total of 17 runs were carried out to assess the effect of PEI concentration (4–12 mg/mL), stirring time (1–24 h) and solid–liquid ratio (1:0.3–1:2) on PEI grafting and GA concentration (0.5%–4%), cross-linking time (0.5–2 h) and the solid–liquid ratio (1:0.2–1:0.6) of GA cross-linking, respectively.

Table 1 shows a series of PEI modified sorbents synthesized under different conditions. Based on parameter estimations, the empirical relationship between the response variable and independent variables for PEI grafting can be expressed as Eqs. (1) and (2):

$$Y = 16.57 - 0.49X_1 + 8.89X_2 + 1.75X_3 - 0.10X_1X_2 - 0.03X_1X_3 + 0.19X_2X_3 + 0.14X_1^2 - 4.34X_2^2 - 0.05X_3^2 \quad (1)$$

where Y is the adsorption capacity of the MO solution, and X_1, X_2, and X_3 represent the values of PEI concentration, solid–liquid ratio and stirring time.

For the GA cross-linking process, the empirical relationship between the response variable and independent variables can be expressed as

$$Y = 40.34 + 2.05X_1 - 8.71X_2 + 5.53X_3 + 7.31X_1X_2 - 0.91X_1X_3 - 1.14X_2X_3 - 0.12X_1^2 + 8.10X_2^2 - 1.85X_3^2 \quad (2)$$

where Y is the adsorption capacity of the MO solution, and X_1, X_2, and X_3 represent the values of GA concentration, solid–liquid ratio and cross-linking time.

2.5. Adsorption and desorption experiments

Isotherm and kinetic batch experiments were performed to evaluate the sorption performance of KF-DOPA-PEI/GA in MO solution with an initial pH value. The adsorption kinetic assays were carried out with contact times ranging from 0 to 4 h at 28°C, using an initial MO concentration of 50 mg/L and KF-DOPA-PEI/GA concentration of 0.4 g/L. The adsorption isotherm studies were carried out using different concentrations of MO ranging from 25 to 500 mg/L at initial pH, while maintaining a KF-DOPA-PEI/GA concentration of 0.4 g/L, contact time of 2 h and temperature of 28°C. The effect of pH (ranging from 2 to 10) was investigated using an initial MO concentration of 50 mg/L. For desorption assessment, 0.02 g of KF-DOPA-PEI/GA was initially added to 50 mL of MO solution (50 mg/L) and left for 2 h at 28°C. After the adsorption was complete and the supernatant was decanted, the MO-loaded adsorbent was washed with DW and then mixed with 30 mL 0.5 M HCl solution for 1 h. It was then dried in a vacuum and stored for further use.

After each test, the adsorbent was separated from the solution using a 0.45 μm polypropylene syringe filter. The filtrate was diluted with DW and analyzed by measuring absorbance at 464 nm. Adsorption capacities (mg/g) were calculated as per Eq. (3):

$$Q_e = \frac{C_0 - C_t}{M} V \tag{3}$$

where C_0 and C_t are the initial and residual concentrations (mg/L) of the MO solution, respectively, and M (g) and V (L) are the weight of bioabsorbent (0.02 g) and volume of solution (50 mL), respectively.

3. Results and discussion

3.1. BBD for PEI grafting and GA cross-linking

Table 2 presents BDD data on the effect of three independent variables evaluated on the value of Q_e. Statistical significances of the main, interaction and quadratic effects of all variables were predicted by analysis of variance (ANOVA). The statistical significances of each variable (p-value), coefficients of determination (R^2) and adjusted coefficients of determination (R^2 adj) are summarized in Table 3.

ANOVA confirms that the model was significant ($p < 0.0001$) and accounts for 85.99% of the variance in adsorption capacity ($R^2 = 0.8599$; Table 3), highlighting the strong relationship between adsorption capacity and the independent variables in PEI grafting. Lack of fit was insignificant to the relationship of the pure error ($p > 0.05$). Based on p-values derived under different parameters, the stirring time (X_3) was the principal factor affecting the process ($P_C < P_B < P_A$).

In the case of GA cross-linking, the model was found to be significant ($p < 0.0001$), indicating similar levels to the PEI grafting. Lack of fit was insignificant to relative to pure error ($p > 0.05$). Based on p-values derived under the different parameters, the interaction between GA concentration (X_1) and solid–liquid ratio (X_2) was significant ($p < 0.01$). In contrast, significant interactions between X_1X_3 and X_2X_3 were not observed ($p > 0.05$). The results demonstrate that the concentration of GA was the principal factor in all conditions tested ($p < 0.0001$), and therefore indicates that the adsorption capacity may be enhanced by reducing the cross-linking time.

Table 1
Experimental design data for the PEI grafting and GA cross-linking on KF

Run	Independent variables					
	For PEI grafting			For GA cross-linking		
	X_1	X_2	X_3	X_1	X_2	X_3
1	8.00	1.15	12.50	2.25	0.40	1.25
2	4.00	1.15	24.00	0.50	0.60	1.25
3	8.00	1.15	12.50	2.25	0.40	1.25
4	8.00	2.00	24.00	2.25	0.60	0.50
5	8.00	0.30	24.00	0.50	0.40	2.00
6	8.00	0.30	1.00	2.25	0.40	1.25
7	8.00	1.15	12.50	2.25	0.20	0.50
8	4.00	1.15	1.00	0.50	0.20	1.25
9	12.00	0.30	12.50	2.25	0.20	2.00
10	12.00	1.15	1.00	2.25	0.40	1.25
11	8.00	1.15	12.50	2.25	0.40	1.25
12	12.00	2.00	12.50	4.00	0.60	1.25
13	4.00	0.30	12.50	4.00	0.40	0.50
14	8.00	1.15	12.50	4.00	0.40	2.00
15	4.00	2.00	12.50	2.25	0.60	2.00
16	8.00	2.00	1.00	4.00	0.20	1.25
17	12.00	1.15	24.00	0.50	0.40	0.50

Table 2
Experimental design data for the PEI grafting and GA cross-linking on KF

Run	Dependent variables	
	Q_e (mg/g)	
	For PEI grafting	For GA cross-linking
1	36.15	49.10
2	36.83	44.33
3	36.15	47.06
4	40.24	51.83
5	37.51	40.92
6	24.55	52.51
7	36.15	46.38
8	24.55	44.33
9	42.97	46.38
10	38.19	49.10
11	45.01	50.47
12	45.01	60.02
13	32.05	57.97
14	45.01	51.15
15	35.46	51.15
16	19.78	49.79
17	44.33	42.97

Table 3
ANOVA table for the response surface quadratic model of the PEI grafting and GA cross-linking on KF

Items	*p*-value	
	For PEI grafting	For GA cross-linking
A-Concentration	0.0112	<0.0001
B-S:L	0.7874	0.0076
C-Time	0.0037	0.1272
AB	0.8785	0.0343
AC	0.4987	0.2608
BC	0.4122	0.8662
A^2	0.3053	0.7177
B^2	0.1782	0.7433
C^2	0.0237	0.3103
Lack of it	0.7033	0.5298
R-Squared	0.8599	0.9328
Adj *R*-Squared	0.6798	0.8464

3.2. Optimization of synthesis using RSM

Three-dimensional response surface plots of PEI grafting assays are shown in Fig. 1. The MO adsorption capacity is clearly dependent on the PEI concentration, solid–liquid ratio and stirring time; this is consistent with the data presented in Table 2. Fig. 1a depicts the three-dimensional response surface relationship of PEI concentration and solid–liquid ratio with regard to MO adsorption at a constant stirring time of 12.5 h. Adsorption capacity (at a PEI concentration of 4 mg/mL) increased from 32.05 to 35.46 mg/g when the solid–liquid ratio was increased from 0.3 to 2. The relationship between the solid–liquid ratio and MO adsorption may correlate with the level of amino functional groups on the surface of the adsorbent. A reduction in amino functional groups is thought to result in a decrease in adsorption capacity. Accordingly, suitable cross-linking degrees should be controlled for the solid–liquid ratio. The MO adsorption capacity increased from 32.05 to 42.97 mg/g (at a solid–liquid ratio of 0.3) when PEI concentration was increased from 4 to 12 mg/mL. This indicates that a high PEI concentration enhances the adsorption capacity of the modified KFs through the induction of amino groups. Additionally, the MO adsorption capacity increased from 24.55 to 36.83 mg/g (at a PEI concentration of 4 mg/mL and constant solid–liquid ratio of 1.15) when the stirring time was raised from 1 to 24 h (Fig. 1b). This may be due to the PEI layer becoming more stable with a longer stirring time, leading to an increase in adsorption capacity. These findings were similar to the assessment of the effects of solid–liquid ratio and

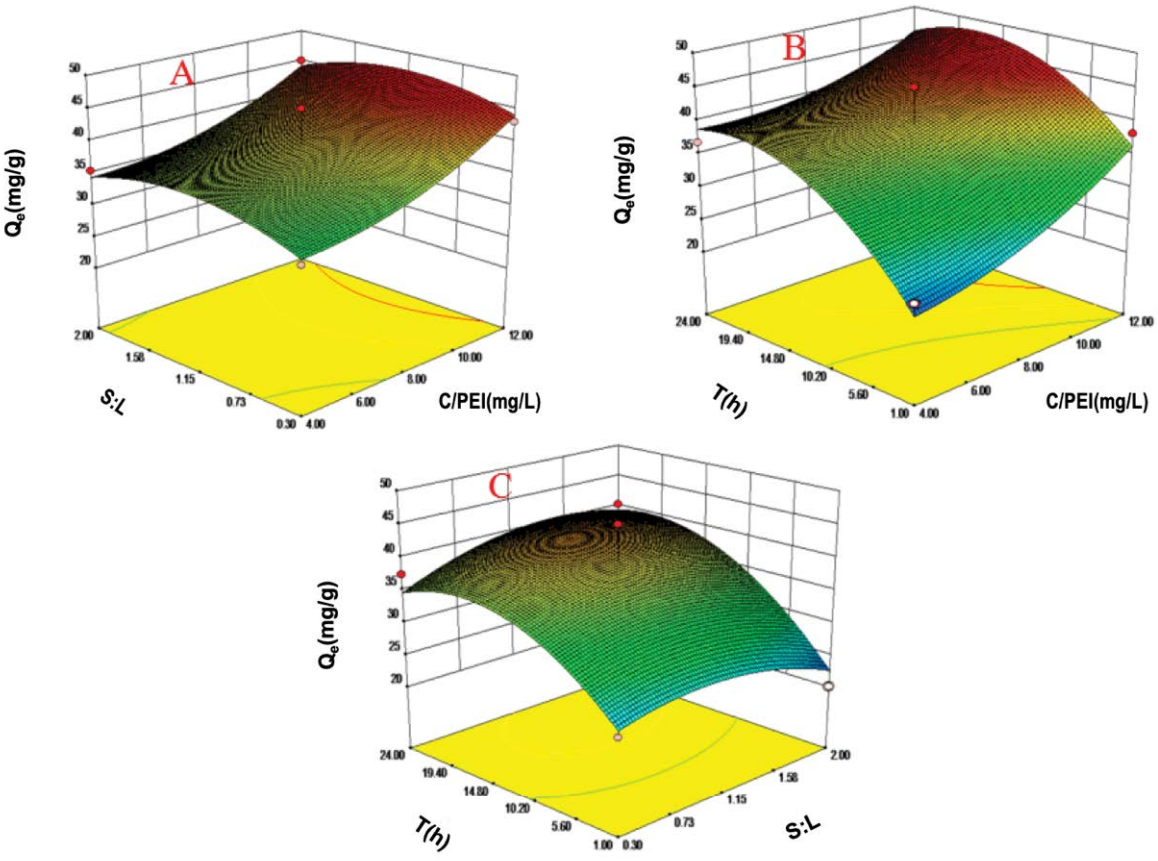

Fig. 1. Response surface plots for the PEI grafting on KF-DOPA for significant interaction effects for MO adsorption. (a) PEI concentration and solid–liquid ratio effect on MO adsorption, (b) PEI concentration and stirring time effect on MO adsorption and (c) Solid-liquid ratio and stirring time effect on MO adsorption.

stirring time (Fig. 1c). PEI concentration, solid–liquid ratio and stirring time appear to influence the adsorption capacity of the absorbent. Based on these observations, optimum conditions for PEI modified KF-DOPA were achieved.

The optimum modification conditions for PEI grifting (Fig. 1) are as follows: PEI concentration of 12 mg/mL, solid–liquid ratio of 1.27 and stirring time of 17.46 h. Using these parameters, the maximum adsorption capacity for the MO solution (48.28 mg/g) was obtained for PEI modified KF-DOPA, which was subsequently used for GA cross-linking analyses.

The effects of GA concentration, solid–liquid ratio and cross-linking time on MO adsorption are shown in Fig. 2. MO adsorption capacity is clearly sensitive to GA concentration, solid–liquid ratio and cross-linking time, and is consistent with the findings presented in Table 2.

Fig. 2a shows a three-dimensional response surface relationship between GA concentration and solid–liquid ratio for the MO adsorption of optimized KF-DOPA-PEI. Adsorption capacity increased from 44.33 to 60.02 mg/g (at a solid–liquid ratio of 0.6 and constant cross-linking time of 1.25 h) when GA concentration was raised from 0.5% to 4%. Moreover, adsorption capacity was found to increase from 49.79 to 60.02 mg/g (under equivalent GA concentrations and a constant cross-linking time of 1.25 h) when the solid–liquid ratio was raised from 0.2 to 0.6. This indicates that a greater GA concentration leads to an improvement in MO adsorption. The substantial increase in MO removal due to a high GA concentration and solid–liquid ratio may be attributed to a significant change in the process of cross-linking. Based on the Schiff-base reaction, the $–NH_2$ and –CHO present in PEI and GA generate C=N that may strengthen the cross-linking and expose the adsorption sites. From the data presented in Figs. 2b and c, we conclude that the MO adsorption capacity decreased from 57.97 to 51.15 mg/g (at a constant GA concentration and solid–liquid ratio) when cross-linking time was increased from 0.5 to 2 h, possible due to the covering of PEI amine ions by GA.

The optimum modification conditions for GA cross-linking were as follows: GA concentration of 4%, solid–liquid ratio of 0.6 and cross-linking time of 0.5 h. The MO adsorption capacity of KF-DOPA-PEI prepared under optimum conditions with GA cross-linking was found to be 62.75 mg/g, which is extremely close to the predicted value. This optimal version of KF-DOPA-PEI/GA was subsequently used in detailed evaluations of its MO adsorption properties.

3.3. Characterization

During the process of surface modification, the color of the raw KFs gradually changed from bright white to dark gray due to the self-polymerization of dopamine on its

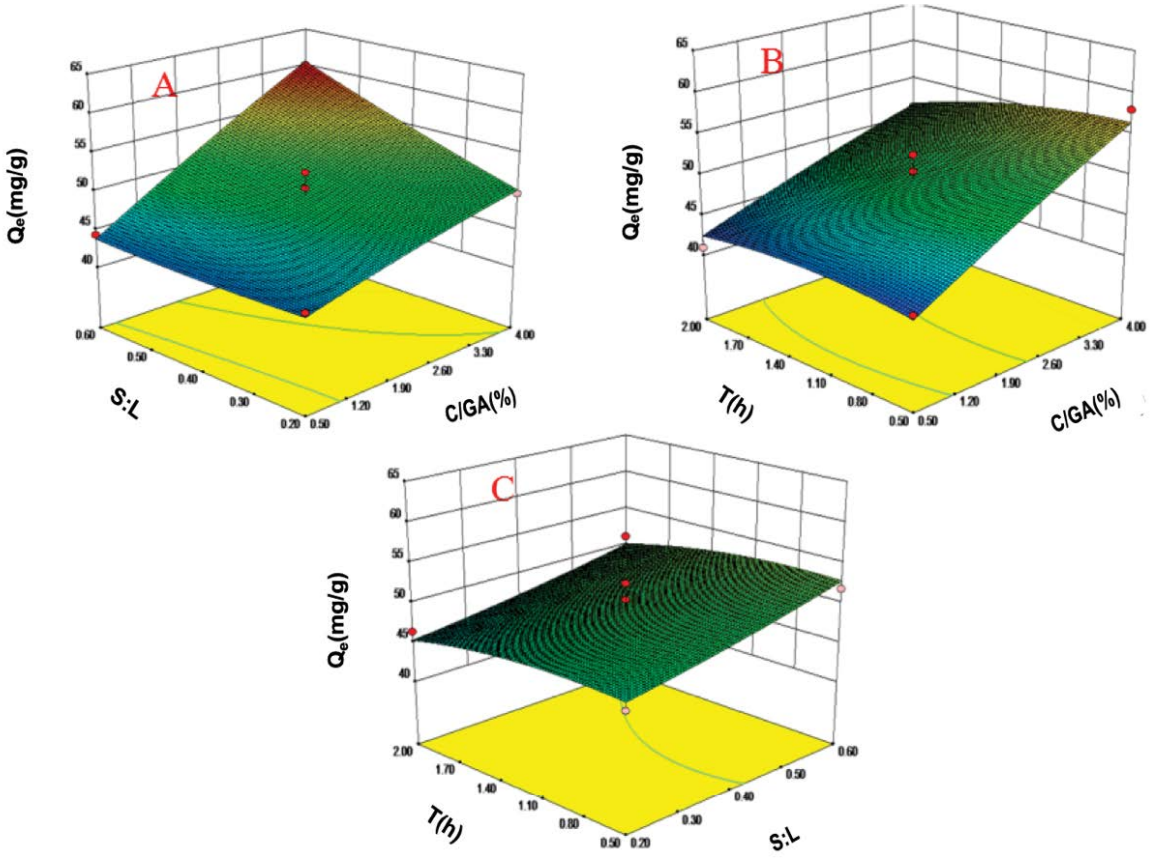

Fig. 2. Response surface plots for the GA cross-linking on KF-DOPA-PEI for significant interaction effects for MO adsorption. (a) GA concentration and solid–liquid ratio effect on MO adsorption, (b) GA concentration and cross-linking time effect on MO adsorption and (c) Solid-liquid ratio and cross-linking time effect on MO adsorption.

surface [30]. After the cross-linking process, the color of KF-DOPA-PEI/GA had changed from dark gray to brown. Fig. 3 shows FE-SEM images of KF, KF-DOPA and KF-DOPA-PEI/GA. A clean and smooth surface is evident due to the waxy structure of the surface of fiber tubes [31] (Fig. 3a). In contrast, a rough surface with different degrees of wrinkles and grooves was observed with KF-DOPA (Fig. 3b). At the completion of the cross-linking process, the 3D interconnected network of KF-DOPA-PEI/GA was retained (Fig. 3c) and the surface became smoother than that of KF-DOPA. This suggests that the cross-linking process greatly affects the surface morphology of the synthesized adsorbent.

Fig. 4 shows FTIR spectra of KF, KF-DOPA and KF-DOPA-PEI/GA. The strong peak at 3,341 cm^{-1} was assigned to non-free O–H stretching vibrations, while another peak at 2,917 cm^{-1} was identified as asymmetric and symmetric stretching vibrations in $–CH_2$ and $–CH_3$ groups, due to the waxy structure on the surface of the KFs [32]. The absorption peak at 1,738 cm^{-1} relates to the C=O stretching vibration of ketones, carboxylic groups, or esters, and a further peak at 1,035 cm^{-1} was assigned to a carbohydrate. In comparisons with the spectra of KF, significant increases in absorption bands were observed for KF-DOPA and KF-DOPA-PEI/GA. This may be explained by the induced functional groups (e.g., hydroxyl groups, amino groups, carbonyl groups and aromatic rings) from the self-polymerization of dopamine and PEI/GA cross-linking [33], indicating the successful coating of DOPA onto the surface of the KF, and efficient grafting of PEI on the poly-DOPA film.

Change in water contact angles is shown in Fig. 5. During the dopamine-polymerizing process, the hydrophobicity of the raw KF was able to display the hydrophilicity. The water contact angle was reduced from 105.12° to 80.2°. Moreover, KF-DOPA-PEI/GA became more hydrophilic after cross-linking with PEI and GA with a water contact angle of 31.42° (Fig. 5c). The decreased contact angle provides further confirmation that DOPA and PEI successfully grafted onto the surface of the raw KFs. The contrasting wettability of water on the fibers provides a simple basis for adsorption of MO dye in wastewater.

3.4. Effect of solution pH

pH is known to play a critical role in the surface properties and ionization degree of adsorbents, and contaminant speciation during the adsorption process [34]. Fig. 6 shows that the adsorption capacity decreased with an increase in pH from 4 to 10, possibly due to the deprotonation of surface $–NH_3$ and –OH groups. This deprotonation leads to a decrease in the positive potential of KF-DOPA-PEI/GA, thereby reducing its electrostatic interaction with MO [35,36]. On the other hand, the charge on the surface of KF-DOPA-PEI/GA is positive due to protonation of the surface binding. When pH was raised from 2 to 4, the ionization degree of the

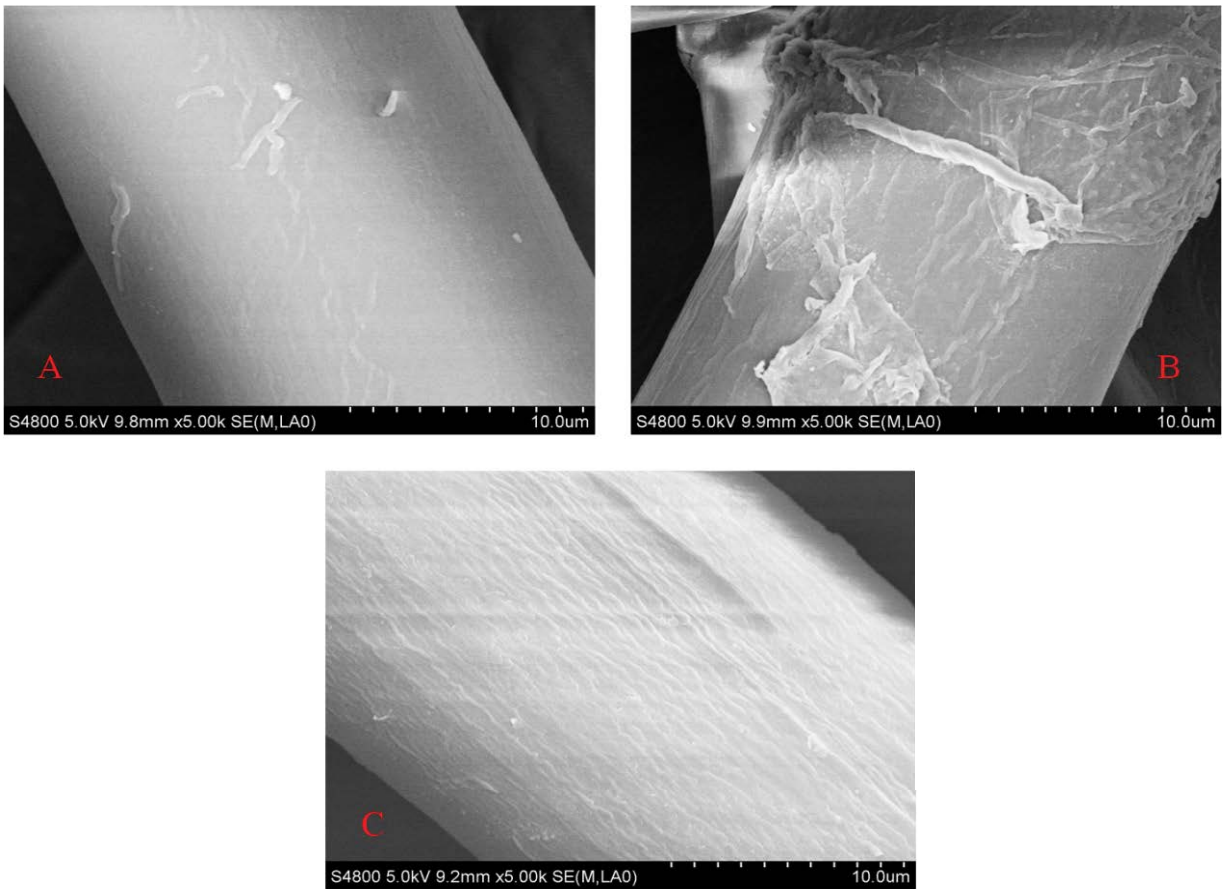

Fig. 3. SEM images of the KF. (a) the raw KF; (b) KF-DOPA and (c) KF-DOPA-PEI/GA.

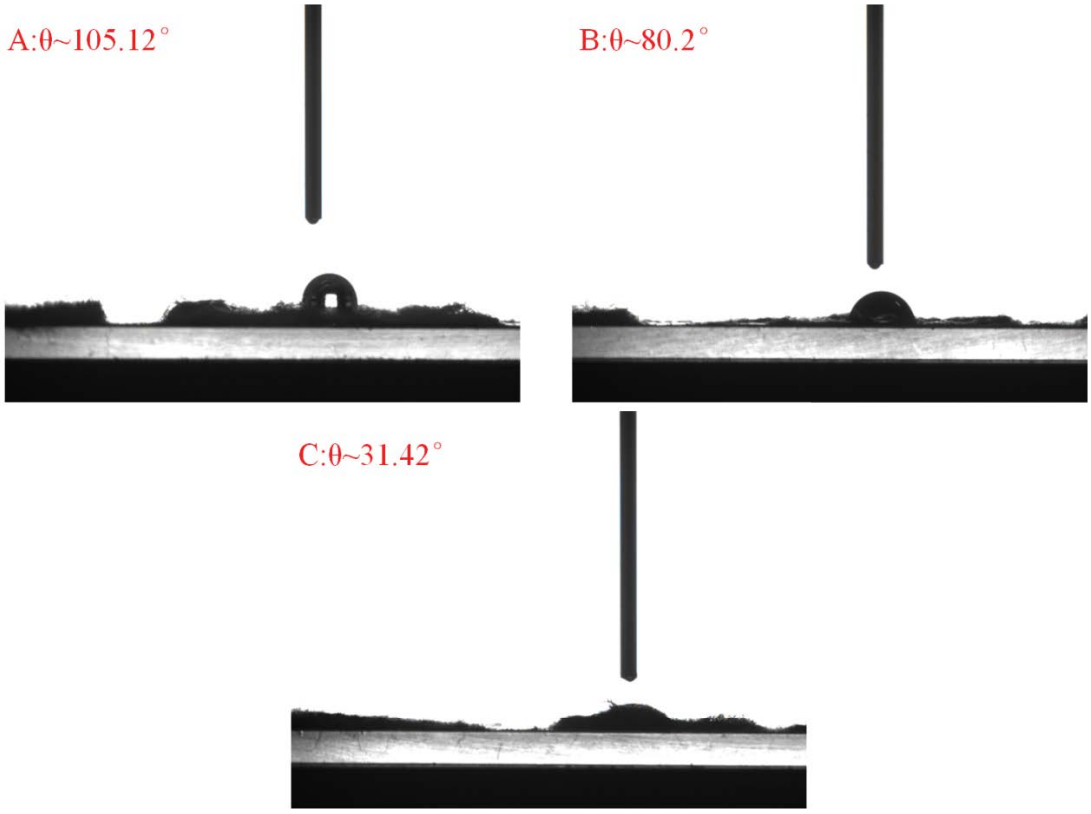

Fig. 4. Water contact angle images of KF. (a) the raw KF, (b) KF-DOPA and (c) KF-DOPA-PEI/GA.

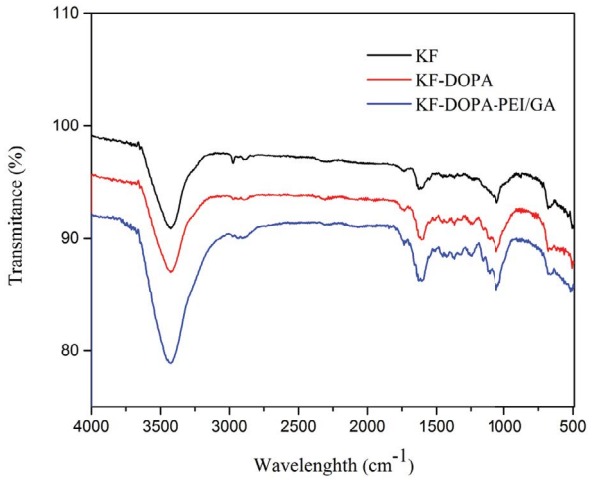

Fig. 5. FTIR spectra of the raw KF, KF-DOPA and KF-DOPA-PEI/GA.

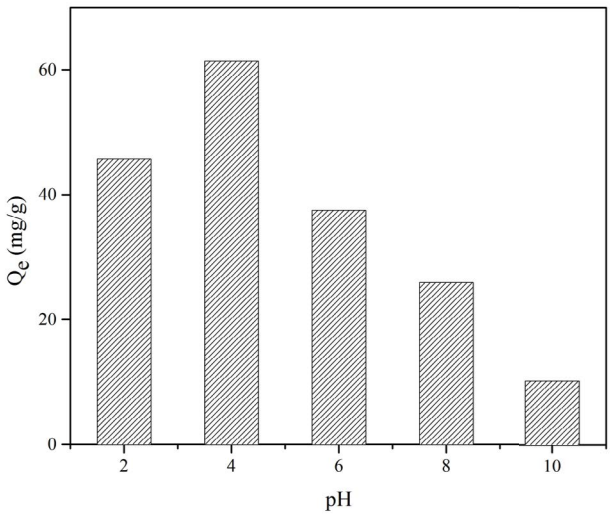

Fig. 6. Effect of the initial solution pH on the adsorption capacity.

MO molecules increased accordingly, due to favorable conditions for electrostatic attraction between $-NH_3^+$ of KF-DOPA-PEI/GA and SO_3^- of MO. Furthermore, MO changed to its cationic form when the pH value was greater than 7, and the electrostatic repulsion force between cationic MO and the positive charge of the adsorption sites led to a decrease in adsorption capacity. Based on these pH experiments, the maximum adsorption capacity was found to be 62.75 mg/g, achieved at a pH of 4.

3.5. Adsorption experiments

Adsorption kinetic analysis is an extremely important concept in water treatment as it depicts the adsorbate uptake rate, which in turn dictates the time taken for adsorbate uptake at the solid–solution interface [37]. The effects of different contact times on adsorption are shown in Fig. 7. The fitting kinetic parameters and adsorption capacities are outlined in Table 4.

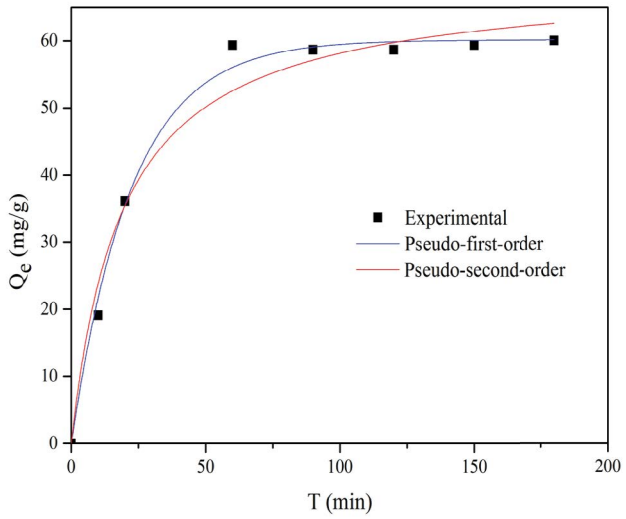

Fig. 7. Kinetic study of KF-DOPA-PEI/GA.

A significant change in the initial slope of adsorption was observed (Fig. 7), confirming a high initial adsorption rate. Indeed, the correlation coefficient of pseudo-first-order kinetics curve (0.994) was superior to that of the pseudo-second-order dynamic curve (0.974). The pseudo-first-order kinetics curve fitted well with the adsorption kinetics of the MO solution, that is, smooth, continuous and linear. KF-DOPA-PEI/GA is a fiber with a huge hollow lumen which provides a site where adsorbate molecules can disperse freely and quickly; accordingly, a PEI polymer was grafted in the KF-DOPA surface. Thus, many positions of activation are available for MO molecules, leading to a high adsorption efficiency. Conversely, KF and KF-DOPA showed scant adsorption efficiency due to their hydrophobic characteristic.

Adsorption isotherms are used to describe how adsorbates interact with adsorbents, and the constants of isotherm models are useful in determining the concentration of an adsorbent needed to adsorb a defined amount of adsorbate. In the present study, the Langmuir and Freundlich adsorption isotherm model equations were used. The experimental data are shown in Fig. 8, and the fitting isotherm model parameters are summarized in Table 5.

The extent of MO adsorption was significantly influenced by the initial concentration of MO in the solution. Fig. 8 demonstrates that the adsorption capacity of KF-DOPA-PEI/GA increased to a maximum of 85.02 mg/g (as per the Langmuir model) when assays were performed using a range of initial MO concentrations (25 to 500 mg/L).

Table 4
Kinetics parameters for the adsorption MO on KF-DOPA-PEI/GA

Pseudo-first order			Pseudo-second order		
Q_e (mg/g)	K_1 (min^{-1})	R^2	Q_e (mg/g)	K_2 (g/mg min)	R^2
60.14	0.045	0.994	69.22	0.0008	0.974

Furthermore, Langmuir and Freundlich isotherm models were used to evaluate the distribution of MO on the surface of KF-DOPA-PEI/GA after equilibrium was reached at a constant temperature. Generally, the Langmuir isotherm model assumes that only monolayer adsorption takes place on a homogeneous surface, with no interactions between the adsorbate molecules [38]. In contrast, the Freundlich isotherm model describes the adsorption between adsorbate molecules and adsorbents with heterogeneous surfaces. To evaluate the fittings of the two models to the adsorption process, the following linear form of Langmuir and Freundlich [39] equations were adopted as Eqs. (4) and (5) respectively:

$$\frac{C_e}{Q_e} = \frac{C_e}{Q_m} + \frac{1}{Q_m K_L} \tag{4}$$

$$\ln Q_e = \frac{1}{n}\ln C_e + \ln K_F \tag{5}$$

where Q_e (mg/g) and Q_m (mg/g) are the equilibrium adsorption capacity and the maximal adsorption capacity for monolayer adsorption, respectively; C_e (mg/L) is the equilibrium concentration of MO; K_L (L/mg) is the Langmuir constant relating to adsorption heat; K_F [(mg/g)(mg/L)^n] and n are the Freundlich constants relating to adsorption capacity and adsorbent intensity, respectively.

The fitting of the experimental data to these two isotherm models is shown in Fig. 8, while all the parameters are listed in Table 5. According to the linear correlation coefficient R^2 (0.978 > 0.878), the experimental equilibrium data corresponds to the Langmuir model, indicating that MO adsorption is mainly through a single layer process. Once the MO molecules have occupied the active sites on the adsorbent surface, their adsorption is gradually tending to equilibrium. Consequently, a monolayer of immobilized MO ions is formed on the positively charged binding sites of KF-DOPA-PEI/GA [40].

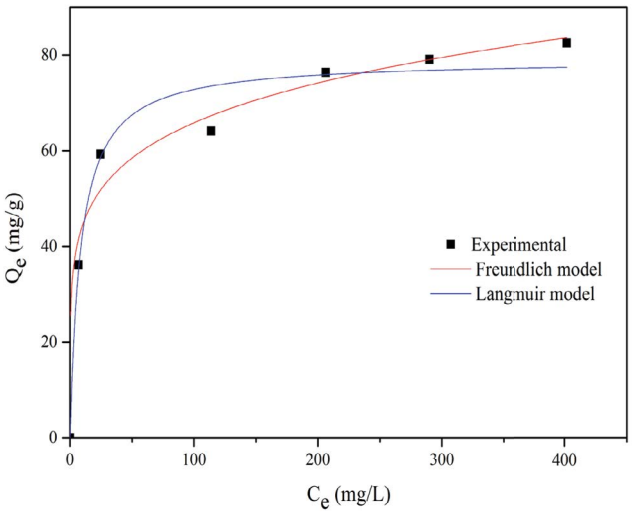

Fig. 8. Adsorption isotherms of KF-DOPA-PEI/GA.

Table 5
Isotherm parameters for the adsorption MO on KF-DOPA-PEI/GA

Langmuir			Freundlich		
Q_m (mg/g)	K_L (L/mg)	R^2	K_F (L/g)	1/n	R^2
85.02	0.034	0.978	21.520	0.223	0.878

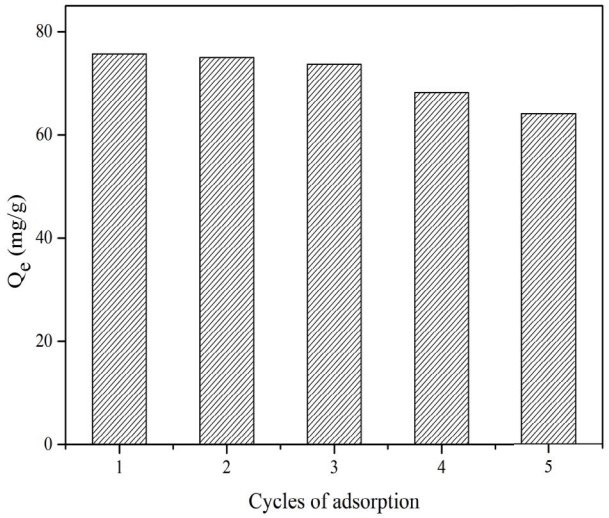

Fig. 9. Reusability of the KF-DOPA-PEI/GA.

3.6. Regeneration studies

Regeneration experiments were conducted to explore the possibility of recycling KF-DOPA-PEI/GA. Fig. 9 illustrates that the regeneration of KF-DOPA-PEI/GA was efficient, with high adsorption capacity remaining even after five regenerations. This may relate to active sites that remain unexposed during repeated adsorption–desorption cycles. Moreover, the desorption efficiency was found to be maintained at 85% after five regenerations. This clearly confirms the high degree of reusability of KF-DOPA-PEI/GA, with the additional advantage of reduced costs.

4. Conclusion

In this study, a novel bioabsorbent KF-DOPA-PEI/GA containing an abundance of ammonium groups was synthesized. This was achieved through layer-by-layer self-assembly of the surface polymerization of DOPA with cross-linked PEI and GA, which resulted in a product capable of removing anionic dyes from water. These results suggest that KF-DOPA-PEI/GA has great potential in the removal of anion dyes during the treatment of wastewater.

Acknowledgments

This work was financially supported by the Shanghai Sailing Program (No.17YF1407200), the "Capacity Building Project of Some Local Colleges and Universities in Shanghai" (No.17030501200) and the National Natural Science Foundation of China (NSFC 21707089).

References

[1] I.M. Lipatova, L.I. Makarova, A.A. Yusova, Adsorption removal of anionic dyes from aqueous solutions by chitosan nanoparticles deposited on the fibrous carrier, Chemosphere, 212 (2018) 1155–1162.
[2] M. Safari, A. Khataee, R. Darvishi Cheshmeh Soltani, R. Rezaee, Ultrasonically facilitated adsorption of an azo dye onto nanostructures obtained from cellulosic wastes of broom and cooler straw, J. Colloid Interface Sci., 522 (2018) 228–241.
[3] X. Yang, Y. Li, H. Gao, C. Wang, X. Zhang, H. Zhou, One-step fabrication of chitosan-Fe(OH)$_3$ beads for efficient adsorption of anionic dyes, Int. J. Biol. Macromol., 117 (2018) 30–41.
[4] M.M. Hassan, C.M. Carr, A critical review on recent advancements of the removal of reactive dyes from dyehouse effluent by ion-exchange adsorbents, Chemosphere, 209 (2018) 201–219.
[5] R.S. Rengasamy, D. Das, C.P. Karan, Study of oil sorption behavior of filled and structured fiber assemblies made from polypropylene, kapok and milkweed fibers, J. Hazard. Mater., 186 (2011) 526–532.
[6] M.M. Rao, D.H. Reddy, P. Venkateswarlu, K. Seshaiah, Removal of mercury from aqueous solutions using activated carbon prepared from agricultural by-product/waste, J. Environ. Manage., 90 (2009) 634–643.
[7] T.M. Yunus Khan, A.E. Atabani, I.A. Badruddin, R.F. Ankalgi, T.K. Mainuddin Khan, A. Badarudin, Ceiba pentandra, *Nigella sativa* and their blend as prospective feedstocks for biodiesel, Ind. Crops Prod., 65 (2015) 367–373.
[8] T. Dong, S. Cao, G. Xu, Highly efficient and recyclable depth filtrating system using structured kapok filters for oil removal and recovery from wastewater, J. Hazard. Mater., 321 (2017) 859–867.
[9] Y. Zheng, J. Wang, Y. Zhu, A. Wang, Research and application of kapok fiber as an absorbing material: a mini review, J. Environ. Sci. (China), 27 (2015) 21–32.
[10] X. Zhang, W. Fu, C. Duan, H. Xiao, M. Shi, N. Zhao, J. Xu, Superhydrophobicity determines the buoyancy performance of kapok fiber aggregates, Appl. Surf. Sci., 266 (2013) 225–229.
[11] N. Ali, M. El-Harbawi, A.A. Jabal, C.Y. Yin, Characteristics and oil sorption effectiveness of kapok fibre, sugarcane bagasse and rice husks: oil removal suitability matrix, Environ. Technol., 33 (2012) 481–486.
[12] G. Thilagavathi, C. Praba Karan, D. Das, Oil sorption and retention capacities of thermally-bonded hybrid nonwovens prepared from cotton, kapok, milkweed and polypropylene fibers, J. Environ. Manage., 219 (2018) 340–349.
[13] M.A. Abdullah, A.U. Rahmah, Z. Man, Physicochemical and sorption characteristics of Malaysian *Ceiba pentandra* (L.) Gaertn. as a natural oil sorbent, J. Hazard. Mater., 177 (2010) 683–691.
[14] T. Dong, F. Wang, G. Xu, Sorption kinetics and mechanism of various oils into kapok assembly, Mar. Pollut. Bull., 91 (2015) 230–237.
[15] S.D. Tigno, M.U. Herrera, M.D.L. Balela, Hydrophobicity of functionalized TiO_2-based kapok nanocomposite, Surf. Coat. Technol., 350 (2018) 857–862.
[16] J. Wang, H. Wang, Eco-friendly construction of oil collector with superhydrophobic coating for efficient oil layer sorption and oil-in-water emulsion separation, Surf. Coat. Technol., 350 (2018) 234–244.
[17] A.C. Lacuesta, M.U. Herrera, R. Manalo, M.D.L. Balela, Fabrication of kapok paper-zinc oxide-polyaniline hybrid nanocomposite for methyl orange removal, Surf. Coat. Technol., 350 (2018) 971–976.
[18] Y. Zheng, Y. Zhu, A. Wang, Kapok fiber structure-oriented polyallylthiourea: efficient adsorptive reduction for Au(III) for catalytic application, Polymer, 55 (2014) 5211–5217.
[19] S. Daneshfozoun, M.A. Abdullah, B. Abdullah, Preparation and characterization of magnetic biosorbent based on oil palm

empty fruit bunch fibers, cellulose and *Ceiba pentandra* for heavy metal ions removal, Ind. Crops Prod., 105 (2017) 93–103.
[20] T. He, W. Zhu, X. Wang, P. Yu, S. Wang, G. Tan, C. Ning, Polydopamine assisted immobilisation of copper(II) on titanium for antibacterial applications, Mater. Technol., 30 (2014) 68–72.
[21] A.R. Agcaoili, M.U. Herrera, C.M. Futalan, M.D.L. Balela, Fabrication of polyacrylonitrile-coated kapok hollow microtubes for adsorption of methyl orange and Cu(II) ions in aqueous solution, J. Taiwan Inst. Chem. Eng., 78 (2017) 359–369.
[22] H. Zhu, J. Yuan, J. Zhao, G. Liu, W. Jin, Enhanced CO_2/N_2 separation performance by using dopamine/polyethyleneimine-grafted TiO_2 nanoparticles filled PEBA mixed-matrix membranes, Sep. Purif. Technol., 214 (2019) 78–86.
[23] Y. Liu, K. Ai, L. Lu, Polydopamine and Its Derivative Materials: Synthesis and Promising Applications in Energy, Environmental, and Biomedical Fields, Chem. Rev., 114 (2014) 5057–5115.
[24] V.O. Kollath, S. Mullens, J. Luyten, K. Traina, R. Cloots, Effect of DOPA and dopamine coupling on protein loading of hydroxyapatite, Mater. Technol., 31 (2016) 241–245.
[25] Y. Xiao, W. Huang, K. Xu, M. Li, M. Fan, K. Wang, Preparation of anion exchange membrane with branch polyethyleneimine as main skeleton component, Mater. Des., 160 (2018) 698–707.
[26] T. Aftab, F. Bashir, R.A. Khan, J. Iqbal, Treatment of color through the adsorption efficiency of waste tire-derived char using response surface methodology, Desal. Wat. Treat., 57 (2015) 10324–10332.
[27] J. Hao, W. Zhang, G. Xue, P. Rao, R. Wang, Treatment of distillation residue waste liquid from NPEOs by hydrothermal carbonization process for resource recovery, Desal. Wat. Treat., 125 (2018) 26–31.
[28] E.M. El-Sayed, T.M. Tamer, A.M. Omer, M.S. Mohy Eldin, Development of novel chitosan schiff base derivatives for cationic dye removal: methyl orange model, Desal. Wat. Treat., 57 (2016) 22632–22645.
[29] P. Zhao, M. Xin, M. Li, J. Deng, Adsorption of methyl orange from aqueous solution using chitosan microspheres modified by β-cyclodextrin, Desal. Wat. Treat., 57 (2015) 11850–11858.
[30] R. Wang, C.h. Shin, S. Park, L. Cui, D. Kim, J.-S. Park, M. Ryu, Enhanced antibacterial activity of silver-coated kapok fibers through dopamine functionalization, Water Air Soil Pollut., 226 (2015) 2241.
[31] J. Wang, A. Wang, W. Wang, Robustly superhydrophobic/superoleophilic kapok fiber with ZnO nanoneedles coating: Highly efficient separation of oil layer in water and capture of oil droplets in oil-in-water emulsions, Ind. Crops Prod., 108 (2017) 303–311.
[32] O.K. Sunmonu, D. Abdullahi, Characterization of Fibres from the Plant *Ceiba Pentandra*, J. Text. Inst., 83 (1992) 273–274.
[33] R. Wang, C.H. Shin, Y. Chang, D. Kim, J.S. Park, Aqueous antibacterial enhancement using kapok fibers chemically modified in 3-D crosslinked structure, Water Environ. Res., 88 (2016) 611–616.
[34] X. Li, Z. Wang, J. Ning, M. Gao, W. Jiang, Z. Zhou, G. Li, Preparation and characterization of a novel polyethyleneimine cation-modified persimmon tannin bioadsorbent for anionic dye adsorption, J. Environ. Manage., 217 (2018) 305–314.
[35] V.S. Munagapati, D.-S. Kim, Adsorption of anionic azo dye Congo Red from aqueous solution by Cationic Modified Orange Peel Powder, J. Mol. Liq., 220 (2016) 540–548.
[36] L. Zhai, Z. Bai, Y. Zhu, B. Wang, W. Luo, Fabrication of chitosan microspheres for efficient adsorption of methyl orange, Chin. J. Chem. Eng., 26 (2018) 657–666.
[37] Y. Jiang, B. Liu, J. Xu, K. Pan, H. Hou, J. Hu, J. Yang, Cross-linked chitosan/beta-cyclodextrin composite for selective removal of methyl orange: adsorption performance and mechanism, Carbohydr. Polym., 182 (2018) 106–114.
[38] C. Duan, N. Zhao, X. Yu, X. Zhang, J. Xu, Chemically modified kapok fiber for fast adsorption of Pb^{2+}, Cd^{2+}, Cu^{2+} from aqueous solution, Cellulose, 20 (2013) 849–860.
[39] J. Yan, X. Li, F. Qiu, H. Zhao, D. Yang, J. Wang, W. Wen, Synthesis of β-cyclodextrin–chitosan–graphene oxide composite and its application for adsorption of manganese ion (II), Mater. Technol., 31 (2016) 406–415.
[40] A.M. Zayed, M.S.M. Abdel Wahed, E.A. Mohamed, M. Sillanpää, Insights on the role of organic matters of some Egyptian clays in methyl orange adsorption: isotherm and kinetic studies, Appl. Clay Sci., 166 (2018) 49–60.